First-principles study of the interfacial adhesion between SiO_2 and $MoSi_2$

D. E. Jiang[1] and Emily A. Carter[2]
[1]*Department of Chemistry and Biochemistry, Box 951569, University of California, Los Angeles, California 90095-1569, USA*
[2]*Department of Mechanical and Aerospace Engineering and Program in Applied and Computational Mathematics, Princeton University, Princeton, New Jersey 08544-5263, USA*

(Received 17 May 2005; revised manuscript received 9 August 2005; published 10 October 2005)

Upon oxidation, a silica scale forms on $MoSi_2$, a potential high-temperature coating material for metals. This silica scale protects $MoSi_2$ against high-temperature corrosive gases or liquids. We use periodic density functional theory to examine the interface between SiO_2 and $MoSi_2$. The interfacial bonding is localized, as evidenced by an adhesion energy that changes only slightly with the thickness of the SiO_2 layer. Moreover, the adhesion energy displays a relatively large (0.40 J/m^2) variation with the relative lateral position of the SiO_2 and $MoSi_2$ lattices due to changes in Si-O bonding across the interface. The most stable interfacial structure yields an ideal work of adhesion of 5.75 J/m^2 within the local density approximation (5.02 J/m^2 within the generalized-gradient approximation) to electron exchange and correlation, indicating extremely strong adhesion. Local densities of states and electron density difference plots demonstrate that the interfacial Si-O bonds are covalent in character. Mo-O interactions are not found in the $SiO_2/MoSi_2$ interface investigated here. Our work predicts that the SiO_2 scale strongly adheres to $MoSi_2$, and further supports the potential of $MoSi_2$ as a high-temperature structural material and coating.

DOI: 10.1103/PhysRevB.72.165410 PACS number(s): 68.35.−p, 71.15.Mb, 73.20.−r

I. INTRODUCTION

High-temperature structural materials and coatings have important applications in aerospace, energy, and other industries.[1] The need to boost the energy efficiency and performance of gas turbine engines requires structural materials able to operate at higher temperatures. Nickel-based superalloys have long been used as the base materials for gas turbine engines. However, their working temperature is usually lower than 1100 °C. Even with inside air cooling and thermal barrier coatings, the highest working temperature that has been achieved for nickel-based superalloys is 1300 °C at best.[2] There is a need to move to even higher temperatures in the future.

$MoSi_2$ offers the potential as both a high-temperature structural material[3] and a high-temperature coating for industrial and military applications.[4] It has a high melting point (2030 °C), high-temperature oxidation resistance, and a brittle-to-ductile transition in the range of 1000 °C to 1400 °C.[5–10] Although $MoSi_2$ was first discovered in 1907 when it was tested for use as a high-temperature protective coating against corrosion for ductile metals,[11] the improvement of $MoSi_2$ for use as a structural material or coating is still actively pursued today.[12] In addition to experimental characterization, the electronic structure and bonding of bulk $MoSi_2$ has been the subject of many density functional theory (DFT) studies.[13–19] In agreement with experiment, $MoSi_2$ was found to be semimetallic, with a pseudogap and a low but nonzero density of states at the Fermi level.

The corrosion resistance of $MoSi_2$ results from a protective silica scale that forms on its surface. The oxidation kinetics and microstructures of the oxides that result depend on temperature, oxygen partial pressure, and $MoSi_2$ particle size.[19–23] By controlling those conditions, a thick protective silica scale can form on the surface of $MoSi_2$ (by the process known as passive oxidation). At an oxidation temperature of ~1200 °C, the silica film tends to be vitreous (amorphous). At higher temperatures, say, 1400 °C, small inclusions of crystalline cristobalite begin to grow out of the amorphous silica (a-SiO_2).[22,24]

Strong adhesion of SiO_2 to $MoSi_2$ may increase the mechanical and thermal stability of $MoSi_2$ as a protective coating for metal substrates. For example, we investigated[25] the adhesion between $MoSi_2$ and Fe using DFT within the generalized gradient approximation (GGA) to electron exchange and correlation. Strong adhesion is found to exist between $MoSi_2$ and Fe (ideal work of separation =3.85 J/m^2). In the current work, we explore the structure, bonding, and energetics of the $SiO_2/MoSi_2$ interface in order to further determine the stability of a multilayer protective coating based on $MoSi_2$. The rest of the paper is organized as follows. We give calculational details in Sec. II, followed by results and discussion in Sec. III, and we summarize and conclude in Sec. IV.

II. CALCULATIONAL DETAILS

We performed DFT calculations[26,27] within both the local density approximation (LDA) and the GGA for electron exchange and correlation, using the Vienna *ab initio* simulation package.[28,29] We employed Blöchl's all-electron projector augmented wave (PAW) method,[30] as implemented by Kresse and Joubert,[31] within the frozen core approximation. We used the standard version of the PAW potentials for Mo, Si, O, and H supplied with VASP for both the LDA and the PBE form of the GGA.[32] A Gaussian smearing method[33] was used for the Fermi-surface smearing, with a width of 0.1 eV. The force tolerance for structural relaxation was set to 0.025 eV/Å.

We tested k-point sampling and kinetic energy cutoff convergence for bulk, surface, and interface supercells. As a result, we used a kinetic energy cutoff of 450 eV for all calculations, which converged the total energy of $MoSi_2$ and SiO_2 to within 1 meV/atom. We used a converged $12\times12\times6$ k-mesh for the orthorhombic unit cell of $MoSi_2$ (see Sec. III A).

Given that the DFT method we employ utilizes periodic boundary conditions, we cannot realistically model the amorphous SiO_2 (a-SiO_2) scale that forms from first principles. Instead we choose a crystalline phase that is structurally similar to a-SiO_2. Neutron diffraction studies have shown that β-cristobalite and a-SiO_2 have a very similar local structure.[34–36] Moreover, they also have similar densities and refractive indexes. We therefore choose β-cristobalite as our model for a-SiO_2. This approach has been adopted by other authors as well.[37–39]

The structure of β-cristobalite has not been uniquely determined and is still controversial. The three structures that have gained the most favor are $Fd3m$, $I\bar{4}2d$, and $P2_13$. We used the $I\bar{4}2d$ structure to model β-cristobalite; the rationale behind this choice will be discussed in Sec. III B. Our structural model for bulk β-cristobalite includes eight SiO_2 units; a $3\times3\times3$ k-mesh was used, which converged the total energy of SiO_2 to within 1 meV/atom.

The ideal adhesion energy is defined as $E_{adh}=(E_1+E_2-E_{12})/A$, where E_1, E_2, and E_{12} are the total energy of the isolated substrate, the isolated coating, and the interface, respectively, and A is the area. To study the $SiO_2/MoSi_2$ interface, we must choose the appropriate surfaces of SiO_2 and $MoSi_2$ to interact. We limit the extent of lattice mismatch[40] to be less than 5%. We examined interfacial matches between $MoSi_2(110)$ or $MoSi_2(001)$ and $SiO_2(100)$ or $SiO_2(111)$. $MoSi_2(110)$ and $MoSi_2(001)$ were examined, since they are the most stable and therefore the most likely to form.[25] Surfaces of a-SiO_2 are poorly characterized experimentally, and modeling a-SiO_2 surfaces with crystallographic surfaces of β-cristobalite has been limited to a few low-index surfaces, mainly, (100) and (111).[37–39,41] We found the best match between $MoSi_2(001)$ and $SiO_2(100)$, with a lattice misfit of only 0.4% for a lateral cell of 50 Å^2, while all other matches have a misfit $>10\%$ for a similar area of lateral cells.

To model $SiO_2(100)/MoSi_2(001)$, we used a 10 Å vacuum layer and a six-layer single-Si-terminated $MoSi_2(001)$ slab, which was previously found experimentally[42] and theoretically[25] to be the lowest energy (001) cleavage plane. The bottom three substrate layers were kept fixed at their bulk positions to model a semi-infinite crystal. Relaxing the fourth layer of substrate atoms changed the total energy by only 1 meV/atom. The top three substrate atoms were allowed to relax together with all atoms in the SiO_2 scale. We varied the thickness of SiO_2 to achieve convergence with respect to adhesion energy (see Sec. III C). A $4\times4\times1$ k-mesh was used for the interface, which converged the adhesion energy to ~0.01 J/m^2. The asymmetric construction of our interfacial slabs might cause an artificial interaction across the vacuum due to the surface dipole. However, we did not bother with a dipole correction since the magnitude of the correction to the total energy was estimated to be small (<10 meV/supercell for the optimized structures).

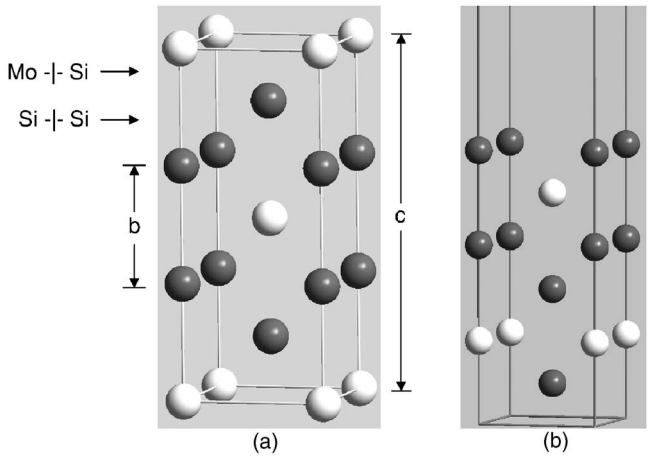

FIG. 1. (a) Bulk structure of $MoSi_2$ and (b) surface structure of single-Si-terminated $MoSi_2(001)$. Si atoms in dark grey and Mo in white.

The same vacuum thickness, k-mesh, and choices of atoms to relax for the interface were also used for the isolated $MoSi_2(001)$ and $SiO_2(100)$ surfaces. The $MoSi_2(001)$ surface was modeled with the same six-layer Si-terminated slab used in the interface calculations. The $SiO_2(100)$ surface was modeled with the same lateral lattice parameters as the $MoS_2(001)$ substrate, again to be consistent with the interface calculations. This causes a very small compressional strain ($\sim0.4\%$) in $SiO_2(100)$, which produced essentially no change in the structural relaxation. The $SiO_2(100)$ surface was terminated with O atoms on both sides when it is first created. For both the isolated surface and the interface slabs, we saturated the O atoms on one side of the $SiO_2(100)$ slab with H atoms, while leaving those on the other side (that will interact with $MoSi_2$) as is. As a result, spin-polarized calculations must be used to study this half-hydrogenated $SiO_2(100)$ surface. For consistency, we therefore used spin-polarized DFT to study $MoSi_2(001)$ and the $SiO_2(100)/MoSi_2(001)$ interface as well.

III. RESULTS AND DISCUSSION

A. Bulk and surface properties of $MoSi_2$

$MoSi_2$ has a body-centered tetragonal structure (C11b), as shown in Fig. 1(a), where an Mo layer is sandwiched by two Si layers. To benchmark our level of theory, we display results for the structural properties of bulk $MoSi_2$ in Table I. We see that PAW-PBE gives reasonably accurate lattice parameters and bulk modulus compared with experiment. PAW-LDA also yields good results, though they are less accurate than those of PAW-PBE, and display the usual consequences of LDA overbinding (shorter lattice constants and larger bulk moduli).

As mentioned in Sec. II, lattice misfit dictates that we study only the $SiO_2(100)/MoSi_2(001)$ interface, which has

TABLE I. Bulk properties of $MoSi_2$: lattice parameters for the tetragonal cell (a, b, and c) and bulk modulus (B). [See Fig. 1(a) for the definitions of a, b, and c.]

Method	a (Å)	b (Å)	c (Å)	B (GPa)
PAW-LDA	3.175	2.562	7.778	229
PAW-PBE	3.215	2.592	7.865	207
Experiment[a]	3.198	2.618	7.859	210

[a]Room temperature data for lattice parameters (Ref. 44) are extrapolated to 0 K using the coefficient of thermal expansion of $MoSi_2$ at 7×10^{-6} K (Ref. 45).

the best lattice match (misfit only ~0.4%) of all low-index surfaces. We studied $MoSi_2$ surfaces in earlier work.[25] We found that it is much easier to cleave bulk $MoSi_2$ between the Si-Si pair of planes than between the Mo-Si pair of planes [Fig. 1(a)]; in other words, $MoSi_2$(001) is preferentially terminated by a single layer of Si [Fig. 1(b)]. This is exactly what high-resolution core-level and valence-band photoemission experiments have shown.[42] Moreover, no reconstruction has been observed in this Si layer, as determined by low energy electron diffraction.[43] This agrees with our finding that those surface Si atoms have zero local magnetic moment (i.e., there are no unpaired electrons associated with those Si atoms).

B. Bulk and surface properties of SiO_2

When $MoSi_2$ is exposed to an oxidizing environment at elevated temperatures, a thin amorphous silica scale will form on the surface of $MoSi_2$. As mentioned above, the DFT method employed to study condensed matter imposes an artificial periodicity that makes it impossible to realistically model amorphous phases such as a-SiO_2. Instead, we use a crystalline phase (β-cristobalite) that structurally resembles a-SiO_2,[35,36] as discussed above.

Unfortunately, as also mentioned above, the structure of β-cristobalite has not been uniquely determined experimentally.[46–48] The three favorite candidate structures belong to the $Fd3m$, $I\bar{4}2d$, and $P2_13$ space groups.[46,49–51] Their structures are related and can be derived from a common framework. The building blocks for most silica polymorphs are corner-sharing tetrahedral SiO_4 units with Si at the center and O at the corners. The bonding between Si and O is predominantly covalent. The final structure is dictated by the way that those relatively rigid tetrahedral units connect. Recently, various crystalline phases of silica, including the three space groups for β-cristobalite, were studied in detail with DFT within LDA and GGA.[50] This work, as well as two other DFT studies,[46,50,51] worked to elucidate the relative stabilities among those three phases of β-cristobalite. The $Fd3m$ phase is commonly thought of as an average (or "mixed") phase, because it has an unphysical angle of Si-O-Si at 180°. The $I\bar{4}2d$ and $P2_13$ phases have been shown to have similar stability and equations of state.[50] However, in the $P2_13$ phase, there is also a 180° Si-O-Si angle in the unit cell. Therefore, we choose the $I\bar{4}2d$ phase to model β-cristobalite. Again, we note that many others also adopted this structure to model β-cristobalite.[37,38,41]

Table II displays the structural parameters we obtained for β-cristobalite with both PAW-LDA and PAW-PBE. Compared with experiment, we see that DFT-LDA generally performs slightly better than DFT-GGA (aside from the c/a ratio). DFT-LDA is especially superior for the equilibrium volume. This has been shown to be true for other phases of SiO_2 as well[50] and our results agree with previous DFT studies.[46,50,51]

Due to its excellent lattice match to $MoSi_2$(001), we use the (100) surface of β-cristobalite to construct the $SiO_2/MoSi_2$ interface. Figure 2 shows the relaxed structure for this surface, where we have modeled a thin film with a structurally converged thickness of three O-Si-O layers. Since surface energy is not well defined for a SiO_2 surface, especially when it is saturated with hydroxyl groups, here we estimated the converged thickness by comparing the relaxed structures at different thicknesses. We found that a SiO_2 slab of three O-Si-O layers has a similar structure to a slab of four or five O-Si-O layers, indicating that even a slab of three O-Si-O layers can well represent a thin film of SiO_2. As mentioned above, the upper surface is terminated with H atoms (i.e., it is saturated with OH groups) and is exposed to vacuum. From the side view [Fig. 2(a)], we see that each of the Si atoms at the upper surface is saturated with two hydroxyl groups, forming so-called geminal silanols. One-half of these OH groups point their H atoms to O atoms on other silanols, to form hydrogen bond chains on the surface [Fig. 2(b)], while the H atoms from the other half of the OH groups are pointed out of the surface. These types of hydrogen bonding networks at β-cristobalite surfaces were discussed in detail in two earlier studies, one employing the Hartree-Fock method[37] and the other using DFT-BLYP.[41] Our surface structure is similar to both of theirs. The bottom surface in our structure is comprised of O atoms each with one unpaired electron. Those dangling bonds remain after

TABLE II. Lattice constants a and c, equilibrium volume (V_{eq}), Si-O bond length, and bond angles for β-cristobalite, assuming the $I\bar{4}2d$ structure.

Method	a (Å)	c/a	V_{eq} (Å^3/SiO_2)	Si-O (Å)	O-Si-O (°)	O-Si-O (°)	Si-O-Si (°)
PAW-LDA	7.07	1.030	45.50	1.608	108.6	111.1	147.9
PAW-PBE	7.19	1.016	48.60	1.626	108.8	110.9	152.7
Experiment[a]	7.13	1.0	45.33	1.611	107.8	112.9	146.7

[a]Reference 52.

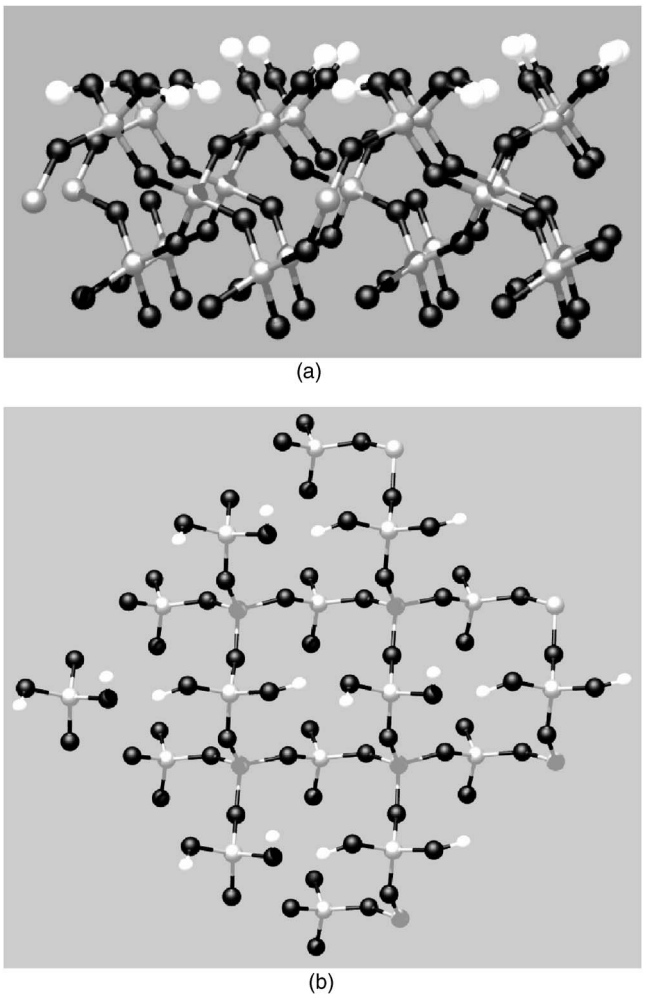

FIG. 2. Side view (a) and top view (b) of the β-cristobalite (100) surface. H atoms are in white, Si in grey, and O in black. The bottom of the surface with unsaturated O atoms is used to adhere to the $MoSi_2(001)$ substrate.

structural relaxation, and they will interact with the surface Si layer of $MoSi_2(001)$ [Fig. 1(b)], as we will discuss next.

C. Adhesion of $SiO_2(100)/MoSi_2(001)$

We investigate how the adhesion energy at the structurally relaxed $SiO_2(100)/MoSi_2(001)$ interface changes with two variables, thickness of the SiO_2 layer and relative lateral position between the SiO_2 and the $MoSi_2$ slabs. We explored the variation in adhesion energy as a function of structure with DFT-LDA rather than DFT-GGA, because of DFT-LDA's superior structural description of β-cristobalite. We first vary the thickness of SiO_2 for a given lateral position. We find that the adhesion energy changes only slightly ($0.15\ J/m^2$) upon increasing the SiO_2 layer thickness from three Si-O-Si layers up to six, indicating the interfacial bonding is very localized, with little long-range contributions to adhesion.

We then examine how the lateral position affects the adhesion energy. We tested six positions for a converged SiO_2 thickness of three O-Si-O layers, and obtained their corresponding adhesion energies (Fig. 3). We see that the DFT-LDA adhesion energies can be divided into two classes, one centered around $5.4\ J/m^2$ and the other at $\sim 5.8\ J/m^2$. We found that these two classes correspond to two different types of interfacial structures, the former energy is associated with structures as in Fig. 4(a), and the latter with structures like in Fig. 4(b). The major difference between these two structures is that four O atoms of $SiO_2(100)$ are bound to four different Si atoms of $MoSi_2(001)$ in Fig. 4(b), while in Fig. 4(a) there are two O atoms sharing one Si atom from $MoSi_2(001)$. As a result of this O-Si-O bonding configuration in Fig. 4(a), the substrate is significantly distorted compared to bulk $MoSi_2$. It is evident in Fig. 4(a) that the shared Si atom is significantly lifted off the substrate (by ~ 0.7 Å). In Fig. 4(b), we see each of the four O atoms from SiO_2 is on top of a Si atom from $MoSi_2$, forming four interfacial bonds and a less distorted substrate surface, leading to a more

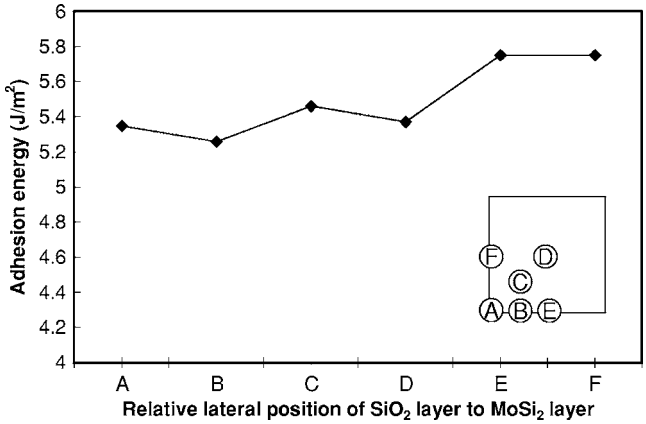

FIG. 3. DFT-LDA adhesion energy vs relative lateral position of the $SiO_2(100)$ film to the $MoSi_2(001)$ substrate, for a three O-Si-O layer thick SiO_2 coating. The inset depicts the lateral cell of the $MoSi_2$ substrate as a square and the positions of the six different translations of the SiO_2 coating, with matching points A–F where A is at (0, 0) and D is at (0.5, 0.5).

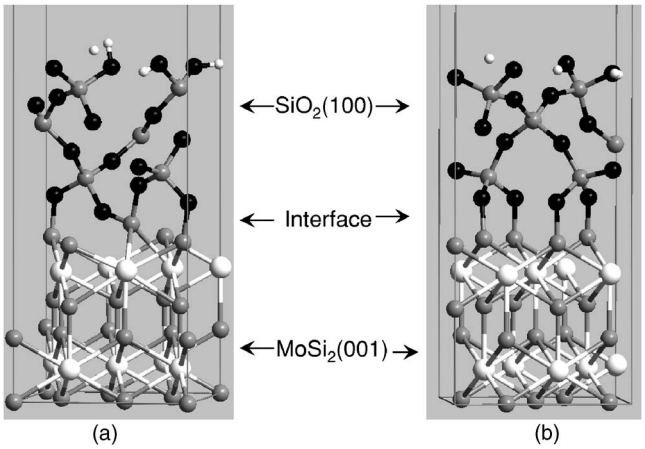

FIG. 4. Two relaxed structures of the $SiO_2(100)/MoSi_2(001)$ interfaces. Large white balls are Mo atoms, small white balls are H. Si atoms are in grey, and O in black. Some H atoms (near the top) may look isolated, but each of them is connected to an O atom in a nearby repeating unit cell.

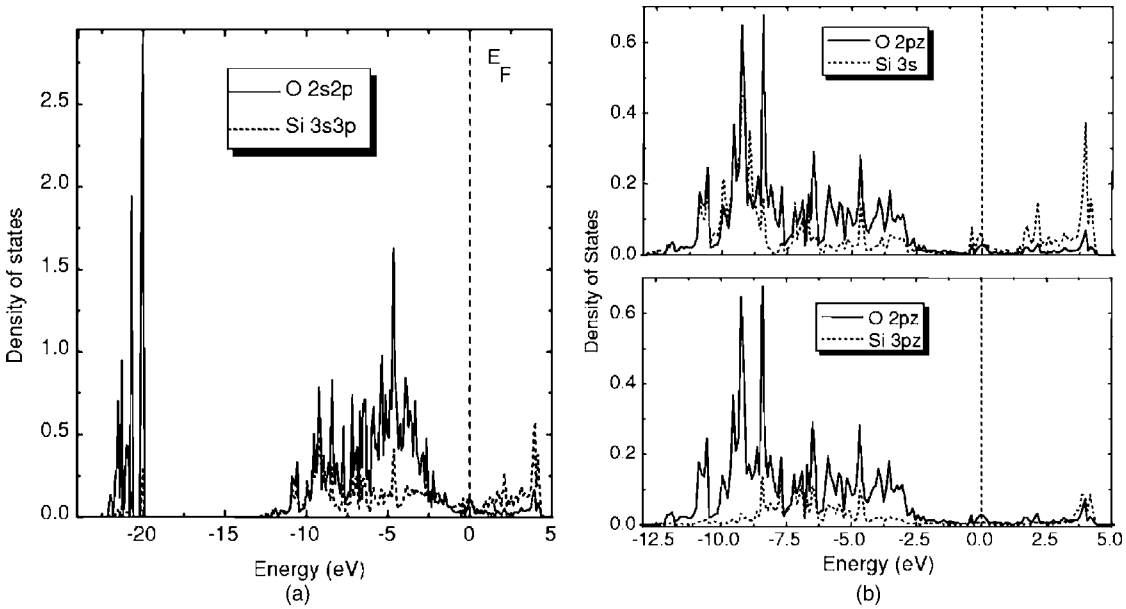

FIG. 5. Site-projected, orbital-resolved local densities of states for Si and O atoms at the $SiO_2(100)/MoSi_2(001)$ interface from Fig. 4(b). The Si atom belongs to $MoSi_2(001)$, while O belongs to $SiO_2(100)$.

stable interface and a higher adhesion energy.

The adhesion energy of 5.75 J/m^2 for the $SiO_2/MoSi_2$ interface was obtained with DFT-LDA, which is likely to be an upper bound, since it is well known that LDA tends to overbind molecules and crystals. Since it is likely then to overbind interfaces, we also optimized this interface with DFT-GGA-PBE, which produces a lower adhesion energy of 5.02 J/m^2. Nevertheless, this adhesion energy (5.02 J/m^2) indicates that the $SiO_2/MoSi_2$ interface is very stable. By comparison, this adhesion energy is higher than the predicted DFT-GGA minimum energy to fracture $MoSi_2$ (i.e., twice the minimum surface energy, $2\gamma[MoSi_2(001)]$) of 4.64 J/m^2, indicating the spallation of silica scale from $MoSi_2$ could be more difficult than the fracture of $MoSi_2$.[25] In earlier work,[25] we obtained a DFT-GGA adhesion energy of 3.85 J/m^2 for $MoSi_2(001)/Fe(100)$, which was considerably higher than other metal-ceramic adhesion energies calculated previously.[40,53–58] Taken together, this suggests that $SiO_2/MoSi_2$ may be a sound coating choice for transition metal substrates.

The lengths of the four interfacial Si-O bonds range from 1.64 to 1.68 Å, close to those in bulk β-cristobalite. Given the covalent nature of the bonding in SiO_2, this suggests a covalent interface may have formed. In order to investigate the bonding further, we display in Fig. 5 the site-projected local density of states (LDOS) for the interfacial Si and O atoms. Figure 5(a) exhibits the Si $3s3p$ and O $2s2p$ states, with O $2s$ states around −22 eV and O $2p$ states centered around −5 eV. We see that strong mixing occurs between O $2p$ and Si $3sp$ occupied states, and the presence of corresponding "antibonding" states above the Fermi level strongly suggests Si-O covalent bonding. Next we resolve the valence band LDOS into angular-momentum-resolved orbital contributions [Fig. 5(b)]. We find that the dominant contribution to the O $2p$ and Si $3sp$ mixing comes from mixing between O $2p_z$ and Si $3s$ [upper panel of Fig. 5(b)], followed by mixing

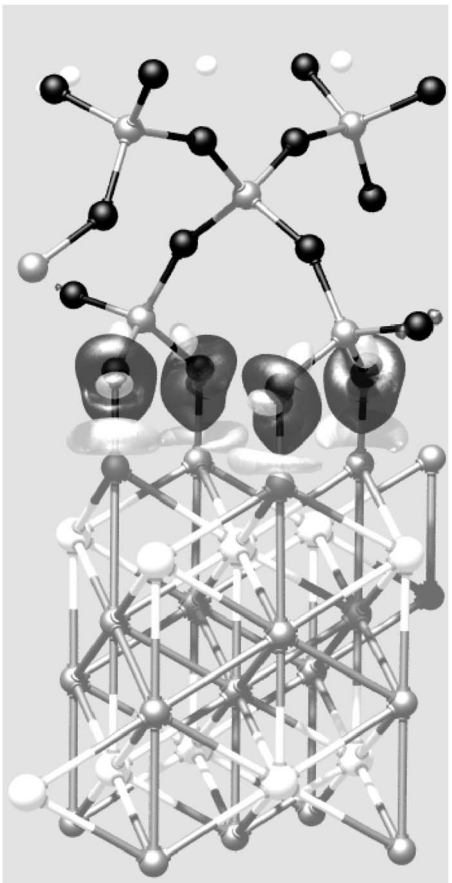

FIG. 6. Isosurface plot of the electron density difference, $\Delta\rho$, for $SiO_2(100)/MoSi_2(001)$ interface. The iso-value is at $-0.075\ e/Å^3$ for the light grey surface and at $0.075\ e/Å^3$ for the dark grey surface. Negative $\Delta\rho$ indicates loss of electron density upon adhesion. Large white balls are Mo atoms, small white balls are H. Si atoms are in grey, and O in black.

between O $2p_z$ and Si $3p_z$ [lower panel of Fig. 5(b)]. The LDOS plots in Fig. 5 are of the interfacial Si and O atoms from Fig. 4(b), where the z axis is along the interface normal. Thus, the interfacial Si-O bonds are formed roughly along the z direction. The strong mixing between Si $3s$ and O $2p_z$, as well as between Si $3p_z$ and O $2p_z$, supports the idea that covalent Si-O bonding leads to strong adhesion between $SiO_2(100)$ and $MoSi_2(001)$. This is further corroborated by the electron density difference plot (Fig. 6), which shows that charge accumulates along Si-O bonds at the interface.

IV. SUMMARY AND CONCLUSIONS

We calculated the properties of an $SiO_2/MoSi_2$ interface using periodic density functional theory with both the local density approximation (LDA) and the PBE form of generalized-gradient approximation (GGA) to electron exchange and correlation. We used the $I\bar{4}2d$ structure of β-cristobalite to model amorphous SiO_2, where the latter is found to form on $MoSi_2$ experimentally. We first explored bulk properties of $MoSi_2$ and SiO_2. We found that both LDA and GGA give satisfactory descriptions of $MoSi_2$ and SiO_2 bulk properties, with LDA offering slightly better structural parameters for β-cristobalite. Among various interfacial matching options, we found the $SiO_2(100)/MoSi_2(100)$ interface has the best match (lattice misfit 0.4% for an area of 50 Å^2). The thickness of the silica layer does not affect the adhesion energy very much, indicating the interfacial bonding is local. Different relative lateral positions lead to two types of interfacial structures, which show a difference of ~ 0.40 J/m^2 in ideal adhesion energy. In the structure with higher adhesion energy, every interfacial O of $SiO_2(100)$ is bound to a different Si atom in $MoSi_2(001)$, while in the structure with lower adhesion energy, two out of four O atoms in the lateral unit cell share one Si atom.

DFT-LDA (GGA) predicts a strong adhesion energy of 5.75 (5.02) J/m^2 for the $SiO_2(100)/MoSi_2(001)$ interface. Strong Si-O bonds are formed across the $SiO_2(100)/MoSi_2(001)$ interface with bond lengths of 1.64–1.68 Å, similar to bulk β-cristobalite. Local densities of states and electron density difference plots show that those interfacial Si-O bonds are covalent in character. In our earlier work, we have shown that $MoSi_2$ adheres strongly to a Fe substrate with an energy of 3.85 J/m^2. By tuning the oxidizing conditions, a protective silica scale can form on $MoSi_2$. Our present work shows that this silica scale adheres even more strongly to $MoSi_2$ than $MoSi_2$ does to Fe, indicating that $MoSi_2$ may indeed be a promising high-temperature coating for steel and other transition metal substrates.

ACKNOWLEDGMENTS

This work was supported by the Army Research Office and the Air Force Office of Scientific Research. The authors thank the Maui High Performance Computing Center and the ARL Major Shared Resources Center for providing CPU time.

[1] National Materials Advisory Board, *Coatings for High-Temperature Structural Materials: Trends and Opportunities* (National Academy Press, Washington, DC, 1996).
[2] N. P. Padture, M. Gell, and E. H. Jordan, Science **296**, 280 (2002).
[3] J. J. Petrovic and A. K. Vasudevan, Mater. Sci. Eng., A **261**, 1 (1999).
[4] T. A. Kircher and E. L. Courtright, Mater. Sci. Eng., A **155**, 67 (1992).
[5] R. M. Aikin, Scr. Metall. Mater. **26**, 1025 (1992).
[6] J. J. Petrovic, MRS Bull. **18**, 35 (1993).
[7] D. J. Evans, F. J. Scheltens, J. B. Woodhouse, and H. L. Fraser, Philos. Mag. A **75**, 1 (1997).
[8] D. J. Evans, F. J. Scheltens, J. B. Woodhouse, and H. L. Fraser, Philos. Mag. A **75**, 17 (1997).
[9] Z. Yao, J. Stiglich, and T. S. Sudarshan, J. Mater. Eng. Perform. **8**, 291 (1999).
[10] R. Mitra, N. E. Prasad, S. Kumari, and A. V. Rao, Metall. Mater. Trans. A **34A**, 1069 (2003).
[11] O. Hoenigsschmid, Monatsch. Chem. **28**, 1017 (1907).
[12] J. K. Yoon, K. H. Lee, G. H. Kim, J. K. Lee, J. M. Doh, and K. T. Hong, J. Electrochem. Soc. **151**, B309 (2004).
[13] B. K. Bhattacharyya, D. M. Bylander, and L. Kleinman, Phys. Rev. B **32**, 7973 (1985).
[14] B. Q. Li, M. R. Ji, J. X. Wu, C. C. Hsu, and J. Yian, Chin. Phys. **10**, 481 (1990).
[15] L. F. Mattheiss, Phys. Rev. B **43**, 12549 (1991).
[16] A. K. McMahan, J. E. Klepeis, M. van Schilfgaarde, and M. Methfessel, Phys. Rev. B **50**, 10742 (1994).
[17] O. K. Andersen, O. Jepsen, V. N. Antonov, B. Y. Yavorsky, A. Y. Perlov, and A. P. Shpak, Physica B **204**, 65 (1995).
[18] Y. Imai, M. Mukaida, and T. Tsunoda, Intermetallics **8**, 381 (2000).
[19] M. Alouani, R. C. Albers, and M. Methfessel, Phys. Rev. B **43**, 6500 (1991).
[20] C. E. Ramberg and W. L. Worrell, J. Am. Ceram. Soc. **85**, 444 (2002).
[21] Y. T. T. Zhu, L. Shu, and D. P. Butt, J. Am. Ceram. Soc. **85**, 507 (2002).
[22] G. Reisel, B. Wielage, S. Steinhauser, I. Morgenthal, and R. Scholl, Surf. Coat. Technol. **146**, 19 (2001).
[23] Y. Q. Liu, G. Shao, and P. Tsakiropoulos, Intermetallics **9**, 125 (2001).
[24] T. A. Kircher and E. L. Courtright, Mater. Sci. Eng., A **155**, 67 (1992).
[25] D. E. Jiang and E. A. Carter, Acta Mater. **53**, 4489 (2005).
[26] P. Hohenberg and W. Kohn, Phys. Rev. **136**, B864 (1964).
[27] W. Kohn and L. J. Sham, Phys. Rev. **140**, A1133 (1965).
[28] G. Kresse and J. Furthmüller, Phys. Rev. B **54**, 11169 (1996).
[29] G. Kresse and J. Furthmüller, Comput. Mater. Sci. **6**, 15 (1996).
[30] P. E. Blöchl, Phys. Rev. B **50**, 17953 (1994).
[31] G. Kresse and D. Joubert, Phys. Rev. B **59**, 1758 (1999).

[32] J. P. Perdew, K. Burke, and M. Ernzerhof, Phys. Rev. Lett. **77**, 3865 (1996).
[33] M. Methfessel and A. T. Paxton, Phys. Rev. B **40**, 3616 (1989).
[34] I. P. Swainson and M. T. Dove, Phys. Rev. Lett. **71**, 193 (1993).
[35] D. A. Keen and M. T. Dove, J. Phys.: Condens. Matter **11**, 9263 (1999).
[36] M. G. Tucker, M. P. Squires, M. T. Dove, and D. A. Keen, J. Phys.: Condens. Matter **13**, 403 (2001).
[37] F. Vigné-Maeder and P. Sautet, J. Phys. Chem. B **101**, 8197 (1997).
[38] D. Ceresoli, M. Bernasconi, S. Iarlori, M. Parrinello, and E. Tosatti, Phys. Rev. Lett. **84**, 3887 (2000).
[39] D. Ricci and G. Pacchioni, Phys. Rev. B **69**, 161307(R) (2004).
[40] A. Christensen and E. A. Carter, J. Chem. Phys. **114**, 5816 (2001).
[41] S. Iarlori, D. Ceresoli, M. Bernasconi, D. Donadio, and M. Parrinello, J. Phys. Chem. B **105**, 8007 (2001).
[42] T. Komeda, T. Hirano, G. D. Waddill, S. G. Anderson, J. P. Sullivan, and J. H. Weaver, Phys. Rev. B **41**, 8345 (1990).
[43] J. P. Sullivan, T. Hirano, T. Komeda, H. M. Meyer, B. M. Trafas, G. D. Waddill, and J. H. Weaver, Appl. Phys. Lett. **56**, 671 (1990).
[44] P. Villars and L. D. Calvert, *Pearson's Handbook of Crystallographic Data for Intermetallic Phases* (American Society for Metals, Metal Park, OH, 1985).
[45] S. D. Conzone, D. P. Butt, and A. H. Bartlett, J. Mater. Sci. **32**, 3369 (1997).
[46] F. Liu, S. H. Garofalini, R. D. King-Smith, and D. Vanderbilt, Phys. Rev. Lett. **70**, 2750 (1993).
[47] I. P. Swainson and M. T. Dove, Phys. Rev. Lett. **71**, 3610 (1993).
[48] F. Liu, S. H. Garofalini, R. D. King-Smith, and D. Vanderbilt, Phys. Rev. Lett. **71**, 3611 (1993).
[49] A. A. Demkov, J. Ortega, O. F. Sankey, and M. P. Grumbach, Phys. Rev. B **52**, 1618 (1995).
[50] T. Demuth, Y. Jeanvoine, J. Hafner, and J. G. Ángyán, J. Phys.: Condens. Matter **11**, 3833 (1999).
[51] L. E. Ramos, J. Furthmuller, and F. Bechstedt, Phys. Rev. B **69**, 085102 (2004).
[52] A. F. Wright and A. J. Leadbetter, Philos. Mag. **31**, 1391 (1975).
[53] W. Zhang and J. R. Smith, Phys. Rev. B **61**, 16883 (2000).
[54] J. R. Smith and W. Zhang, Acta Mater. **48**, 4395 (2000).
[55] D. J. Siegel, L. G. Hector, and J. B. Adams, Phys. Rev. B **67**, 092105 (2003).
[56] S. V. Dudiy, J. Hartford, and B. I. Lundqvist, Phys. Rev. Lett. **85**, 1898 (2000).
[57] A. Arya and E. A. Carter, J. Chem. Phys. **118**, 8982 (2003).
[58] A. Arya and E. A. Carter, Surf. Sci. **560**, 103 (2004).